Građevinski materijali i konstrukcije
Building Materials and Structures
journal homepage: www.buildingmaterialsstructures.com

https://doi.org/10.5937/GRMK2500013L UDK: 624.012.46
691.328.12

Original scientific paper

Poisson's ratio and stress-transfer mechanism of triangular-shaped ten-wire prestressing strand

Žarko Lazić*[1)], Veljko Koković[2)], Snežana Marinković[2)]

[1)] *University of Banja Luka, Faculty of Architecture, Civil Engineering and Geodesy, Banja Luka, Republic of Srpska*
[2)] *University of Belgrade, Faculty of Civil Engineering, Belgrade, Serbia*

Article history
Received: 07 October 2025
Received in revised form: 19 November 2025
Accepted: 01 December 2025
Available online: 16 December 2025

Keywords
Poisson's ratio,
seven-wire strand,
traingular ten–wire strand,
axial strains,
lateral strains

ABSTRACT

This study investigates the Poisson's ratio and deformation behavior of a triangular ten-wire prestressing strand in comparison to conventional seven-wire strand. Experimental tests were conducted under controlled loading to evaluate axial and lateral strains, allowing the determination of strand Poisson's ratios. The results show that ten-wire strands exhibit consistently higher Poisson's ratios (≈0.44) than seven-wire strands (≈0.33), representing an increase of approximately 25% in lateral strain response. This behavior is attributed to the triangular arrangement of wires, which provides additional wire-to-wire contacts and annular spaces, enhancing confinement and strand–concrete interaction. The findings highlight the significant influence of strand geometry on bond efficiency, transfer length, and mechanical response, providing valuable guidance for the design, calibration, and assessment of pretensioned prestressed concrete members. These results support improved predictive modeling of stress transfer and deformation behavior, contributing to more efficient and reliable prestressed concrete design.

1 Introduction

The anchorage and bond behavior of prestressing strands are critically influenced by the Hoyer's effect [1], a phenomenon in which the expansion of the strand under tensile loading enhances the mechanical interlock with surrounding concrete. This expansion is governed by the strand's Poisson's ratio, a material property that directly affects the radial pressure exerted against the concrete and thus plays a central role in the formation and length of the bond transfer zone. While the Hoyer's effect has been extensively considered in traditional analytical models of transfer length, the contribution of the Poisson's effect has rarely been isolated and experimentally quantified, particularly for strands with non-standard geometries. This study aims to investigate the Poisson's coefficient of a conventional 7-wire strand and an innovative 10-wire triangular strand [2, 3] through controlled tensile testing. By evaluating the transverse deformation behavior of both strand types, the study seeks to better understand how strand geometry and Poisson's effect influence the development of bond stress and the effective transfer length in prestressed systems. The results provide insight into the mechanical contribution of the Poisson's effect to the early-age anchorage behavior and can inform refined models for predicting transfer length in emerging prestressing technologies.

2 Background

The main aspects for the theoretical and practical background of this topic are the Hoyer's effect, Poisson's ratio of strand, concrete stress fields in the anchorage zone and transfer length.

2.1 The Hoyer effect

As previously mentioned, one of the primary mechanisms governing bond behavior between prestressing strands and concrete at the ends of pretensioned members is the Hoyer's effect [1].

As the tendon undergoes longitudinal contraction due to stress relief, it simultaneously expands laterally as a result of Poisson's effect. This expansion of the strand generates radial pressure at the strand–concrete interface, increasing mechanical interlock and enhancing bond strength within the transfer zone [1,4,5].

The surrounding concrete resists this transverse expansion, creating a confining pressure that contributes to the development of a radial stress field. This stress field is critical for force transfer from the strand to the concrete over a defined transfer length. The magnitude of the Hoyer's effect, and therefore the bond quality, is influenced by several factors, including the strand diameter, surface geometry (e.g., smooth or indented), and the stiffness of concrete at the time of prestress release [5-7].

* Corresponding author:
E-mail address: zarko.lazic@aggf.unibl.org

The distribution of prestressing force along the transfer length is not uniform. Instead, it decreases progressively toward the free end of the member. As the axial force diminishes, the strand gradually attempts to regain its original (unstressed) diameter. This localized diameter recovery continues to exert radial pressure on the surrounding concrete [4,5], thus maintaining bond strength and contributing to a reduction in the required transfer length (Figure 1).

This localized diameter recovery is connected with the Poisson's ratio of the strand. While typical steel materials exhibit a Poisson'sratio around 0.30 [8], the actual value may vary based on manufacturing processes, residual stresses, and strand geometry. In the case of conventional 7-wire strands, assumptions of constant material properties, including the Poisson's ratio, are embedded in simplified analytical models and code-based transfer length predictions [9-11]. However, these assumptions may not hold for non-traditional strand configurations, such as triangular 10-wire strands, which introduce distinct internal wire arrangements, increased surface area, and potentially different deformation behavior under load.

The influence of strand geometry on the bond performance has been addressed in several studies. Moustafa [12] and Arnold [13] demonstrate that strand surface condition, shape, and confinement directly impact pull-out behavior and bond stress distribution in mortar and concrete. The change in strand surface and wire configuration affects the bond characteristics, emphasizing the importance of contact area and surface deformation in maintaining high bond performance. This highlights that even small variations in geometry can alter the radial stress distribution induced by the Poisson's effect, thereby affecting both the local bond strength and the overall transfer length.
Moreover, modern bond-slip models increasingly recognize the significance of time-dependent and deformation-induced changes in radial stress, including the cyclic contribution of mechanical interlock and friction. While several models

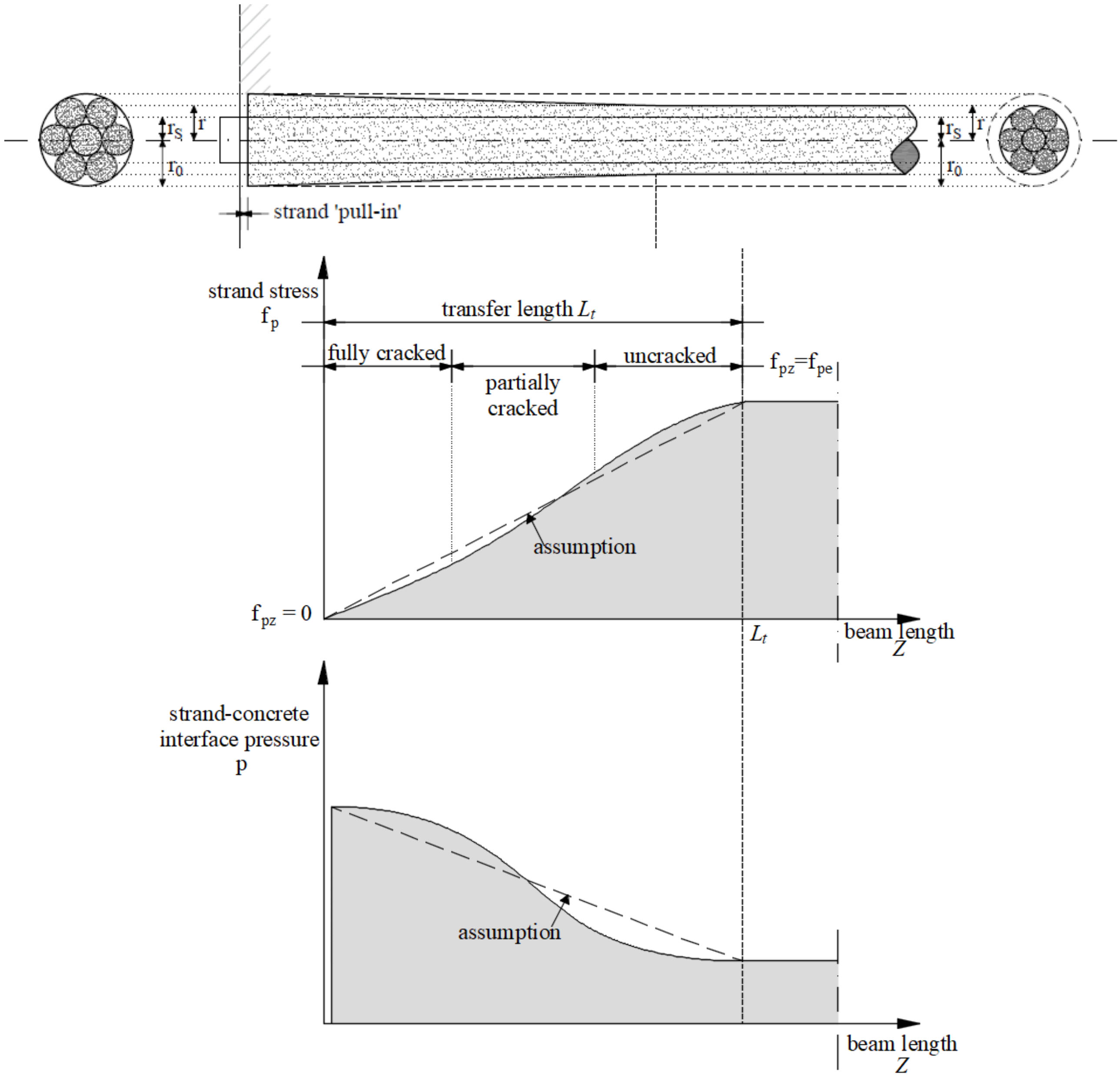

Figure 1. Schematic representation of Hoyer effect along transfer length (based on [4,5])

[11,14] incorporate empirical coefficients to account for strand diameter and concrete strength, they often do not explicitly include the Poisson's ratio as a variable, despite its crucial role in defining radial pressure during initial loading. The general prediction is that strands with different Poisson's ratios will display distinctly different anchorage mechanisms. From this prediction the conclusion is that there is a need for better understanding of this parameter in bond transfer.

Given the emergence of geometrically modified strands, such as the triangular 10-wire configuration, a more comprehensive investigation into the Poisson's effect is warranted. Direct or indirect (Digital image correlation – DIC) experimental measurement of the Poisson's ratio under tensile loading can provide deeper insight into lateral deformation and also how it contributes to anchorage behavior, especially in the early transfer phase. Understanding this relationship is essential not only for improving predictive accuracy of transfer length models but also for validating design codes that still rely on data derived from conventional strand types.

2.2 Poisson's ratio of strand – physical interpretation

Considering a single plain wire, the transfer of prestress force is influenced by the normal stress caused by the wire's radial expansion and the wedge action arising from the transfer of the prestressing force, as illustrated in Figure 1. The Poisson’s ratio for the steel wire is often taken as v_s = 0.27 [5]. For prestressing strands the situation is different, because contraction of strands is not fully described by Poisson’s ratio of steel v_s. The helical outer wires undergo some torsion and tighten when a seven-wire strand is subjected to tension. Initially, they fill any annular space within the strand and then press against each other at their points of contact, Figure 2[5].

The tightening of the strand and the interaction between wires cause strand contraction, in addition to the contraction resulting from the Poisson's effect in each wire. The Poisson's contraction of the individual wires enables the helical wires to tighten further, while the bearing of the outer helical wires on the central straight wire, increases its compression.

Considering the case of a triangular 10-wire strand, the general concept of stress transfer and radial expansion is adopted to be analogous to that of the conventional 7-wire strands. However, the geometric configuration introduces certain distinctions in the way radial stresses are distributed around the strand-concrete interface. The 10-wire strand typically forms an equilateral triangular cross-section, where the outer wires are arranged in a compact triangular pattern surrounding central wires. The characteristic dimension, used to represent the radial expansion of the strand, is taken as the triangle nominal diameter, $2r_0$ (diameter of the circumscribed circle), Figure 2. This substitution was used to enhance clarity in comparison context with conventional circular strand models, where r_0 represents the nominal strand radius.

Despite the geometric difference, the key mechanisms, Poisson's ratio-induced lateral expansion, radial pressure generation, and concrete confinement response, remain fundamentally the same. However, the flat sides and sharper corners of the triangular strand shape may lead to localized variations in radial stress concentrations and bond behavior, particularly near the vertices of the triangular cross-section.

2.3 Concrete stress fields induced by strand anchorage

The development of radial and circumferential stresses was theoretically observed in literature as concrete stress fields. The theoretical analysis of concrete stress fields (induced by Poisson’s ratio of strand), along strand anchorage, was conducted on a single prestressing strand embedded at the center of an isotropic (uncracked) concrete cylinder with a radius of *c* [4]. The value of *c* is considered as the concrete cover distance to the center of the strand. In the simplification, the strand was treated as a solid cylinder with an unstressed radius, r_0, and a stressed radius, r_s (Figure 3).

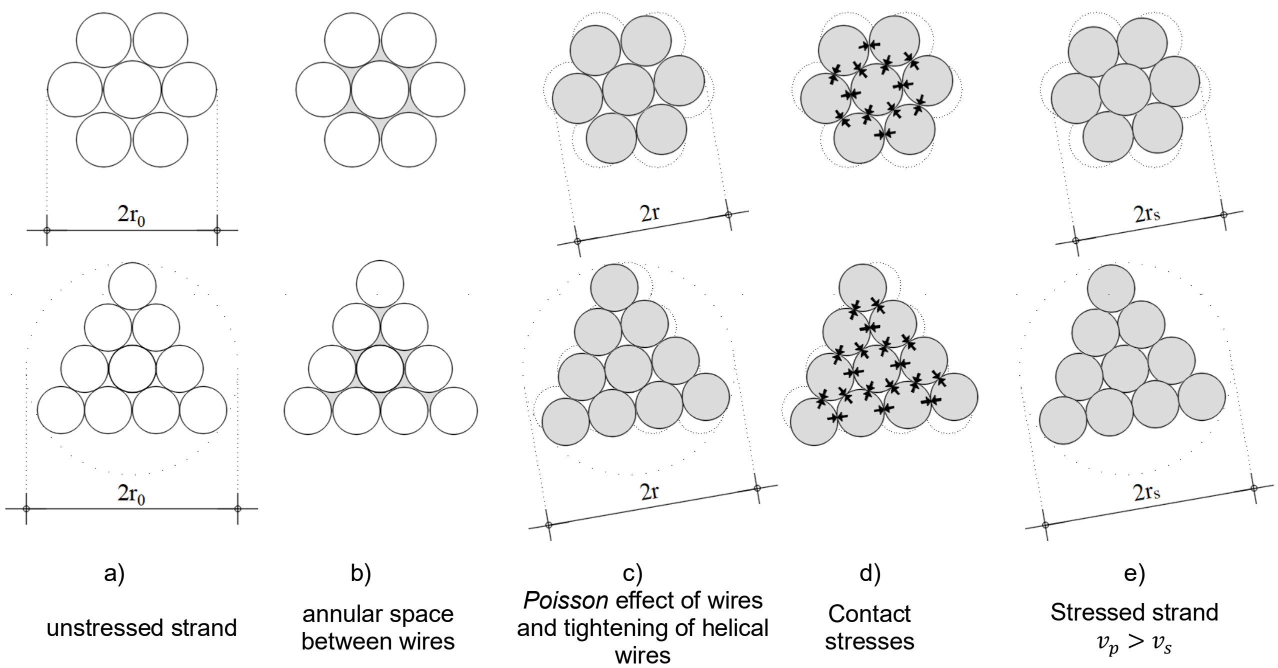

Figure 2. Poisson's ratio of 7-wire and 10-wire prestressing strand (based on [5])

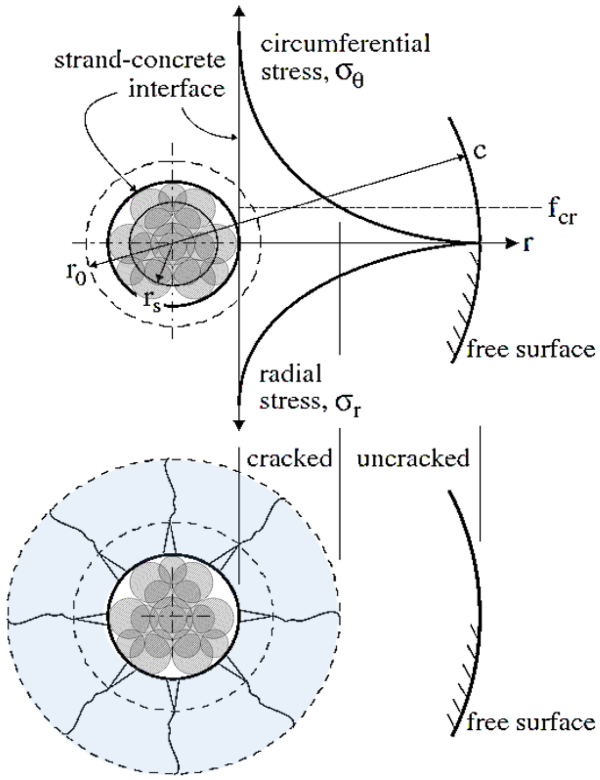

Figure 3. Schematic presentation of stresses and cracking distribution to embedded strand (based on [4,5])

By assuming strain compatibility at the strand - concrete interface, the radial pressure at this interface is determined as [4]:

$$p=\frac{r_o\left(1-v_p f_{pz}/E_p\right)-r_s\left(1-v_c f_{cz}/E_c\right)}{\left(1-v_p\right)r_o/E_p+\left(v_c-(r_s^2+c^2)/(r_s^2-c^2)\right)r_s/E_c}, \quad (1)$$

where r_o- radius of unstressed prestressing strands and r_s- radius of prestressing strands due to initial prestress force f_{pi}:

$$r_s=r_o\left(1-v_p f_{pi}/E_p\right), \quad (2)$$

v_p- *Poisson’s* ratio of prestressing strand, E_p - the Young's modulus of prestressing strand, f_{pz} - the axial stress in prestressing strand at distance ***z*** from the end of the concrete embedment, v_c - the *Poisson's* ratio of concrete, E_c – the Young's modulus of concrete, estimated as: $E_c=4750\sqrt{f_c'}$ (MPa) [11], f_c' - the concrete compressive strength, f_{cz} - the axial stress in concrete at distance ***z*** from the free end: $f_{cz}=f_{pz}r_o^2/c^2$, *c* - radius of concrete cylinder (concrete clear cover + r_0).

The radial and circumferential stresses as functions of the radial distance, *r*, from the strand axis can be determined based on the interface pressure, as described in [4]:

$$\sigma_r=\frac{-p(1/c^2-1/r^2)}{(1/c^2-1/R^2)}, \quad (3)$$

$$\sigma_\theta=\frac{-p(1/c^2+1/r^2)}{(1/c^2-1/R^2)}, \quad (4)$$

where is *R* – the radial distance to the inner boundary of the isotropic (uncracked) region. For an isotropic concrete cylinder, *R* = r_0; this solution is shown schematically in Figure 3 [4]. The stresses at the strand–concrete interface and near the free end of the embedment (***z*** = 0) are significantly high. These high stresses can lead to radial cracking of the concrete, as illustrated schematically in the previous figure. The stress decreases rapidly with increasing radial distance (*r*) from the strand. If the concrete cover is adequate, this will create a cross-section with a cracked zone near the strand and an uncracked annular region surrounding it, where the stresses remain below the concrete's tensile capacity. These regions correspond to anisotropic and isotropic material behavior, respectively, as shown in Figure 3 [4]. The isotropic approach provides sufficient accuracy for determining the probability and extent of cracking related to the anchorage of prestressing strands.

Based on the works of Oh et al. [4] and Briere et al. [5], this approach provides a comprehensive foundation for advancing the modeling and interpretation of prestress transfer mechanisms. While Oh’s model offers a continuum-based representation of bond behavior with an emphasis on axial compatibility and elastic interactions, Briere’s experimental data reveal the critical role of radial mechanics, driven by the Poisson's effect, in establishing initial bond strength. These studies jointly reinforce the need for integrated modeling approaches that account not only for axial stress transfer and bond-slip relationships but also for transverse deformation and confinement effects, particularly in the context of geometrically novel strands such as triangular 10-wire configurations, where the local deformation behavior may deviate significantly from conventional 7-wire strands which may significantly reflect on the transfer length of prestressing force.

2.4 Transfer length

A key factor governing the structural performance of pretensioned members is the efficiency of prestress transfer from the strands to the surrounding concrete.This transfer process is inherently complex and essential, as the prestressing force is reduced to zero at the ends of the member during release, requiring effective anchorage through bond over a defined transfer length [11, 14].

The force equilibrium is set by taking a straight pretensioned strand of nominal diameter $d_b(d_0)$, steel area A_p, effective prestress (steel) stress f_{pe}, when an average bond stress $U_{t,avg}$ acts over a transfer length L_t [15].

$$U_{t,avg} P_p L_t = f_{pe} A_p \tag{5}$$

where,

$U_{t,avg}$ – average bond stress along the transfer length
P_p = $4\pi d_b/3$ – perimeter of prestressing strand (5a)
A_p = $0.725\pi d_b^2/4$– area of prestressing strand (5b)
f_{pe} – effective stress in prestressing strand after all prestress losses.

Rearrange for L_t:

$$L_t = \frac{f_{pe} A_p}{U_{t,avg} P_p} \tag{6}$$

The current equation in the American design code [11] considers only the effects of strand diameter and prestress intensityin the calculation of transfer length in pretensioned members (equation 7):

$$L_t = \frac{f_{pe} d_b}{21} [MPa, mm], \tag{7}$$

where isf_{pe}– effective prestress (after losses) and d_b – the strand diameter.

In the European standard [14], this equation is described in greater detail. The model incorporates the effect of the surrounding concrete's tensile strength, f_{ctd}, which represents the design tensile strength of concrete at the time of release. Additionally, the formulation includes factors that account for strand geometry, bond conditions, and the prestress release method, providing a more comprehensive approach to estimating the transfer length:

$$L_t = \frac{\alpha_1 \alpha_2 f_{pi} d_b}{\eta_p \eta_1 f_{ctd(t)}} [MPa, mm], \tag{8}$$

where is α_1= 1.0 for gradual or α_1= 1.25 for sudden prestress force release, α_2= 0.25 for plain tendons or α_2= 0.19 for 7-wire strand, η_p= 2.7 for indented wires or η_p= 3.2 for 7-wire strand, η_1= 1.0 for good bond condition and η_1= 0.7 otherwise, f_{pi}– prestress force after release.

This approach [14] (equation 8) accounts both concrete cracking behavior (the design tensile strength f_{ctd}(t)) and efficiency of strand anchorage (through the α_2 tendon area parameter).

The tendon area parameter $\alpha_2$respresent:

- For plain tendons (wires):
  - $A_{nominal} = A_{actual} = \pi d_b^2/4$
  - $P_{nominal} = P_{actual} = \pi d_b$

$$\alpha_2 = \frac{A_{actual}}{P_{actual}} \frac{1}{d_b} = \frac{\frac{\pi d_b^2}{4}}{\pi d_b} \frac{1}{d_b} = \frac{d_b}{4} \frac{1}{d_b} = 0.25\,, \tag{9}$$

- For 7-wire strands:
  - $A_{nominal} = 0.78 A_{actual} = 0.78\pi d_b^2/4$
  - $P_{nominal} = \pi d_b$;$P_{actual} = 4\pi d_b/3$

$$adopted\,[14] \rightarrow \alpha_2 = \frac{A_{actual}}{P_{nominal}} \frac{1}{d_b} = \frac{0.78\frac{\pi d_b^2}{4}}{\pi d_b} \frac{1}{d_b} = = \frac{7\text{d}}{36} \frac{1}{d_b} = 0.19\,, \tag{10}$$

$$correct \rightarrow \alpha_2 = \frac{A_{actual}}{P_{actual}} \frac{1}{d_b} = \frac{0.78\frac{\pi d_b^2}{4}}{\frac{4}{3}\pi d_b} \frac{1}{d_b} = = \frac{5.25\text{d}}{36} \frac{1}{d_b} = 0.15. \tag{11}$$

The ratio of transfer length (bond efficiency) calculated using α_2 values for single wires and seven-wire strands is 0.19/0.25 = 0.76. In [5] it was observed that the ratio of Poisson's ratio of a single wire to the Poisson's ratio of seven-wire strand was 0.27/0.4 = 0.68 for 12.7 mm strand and 0.27/0.34 = 0.79 for 15.2 mm strand. Both ratios are very similar, so it is stated that these values are very well reflected with α_2 parameter [5].

3 Objectives

The objectives of the experimental investigation focusing on the Poisson's ratio of 7-wire and triangular 10-wire prestressing strands and the prediction model of triangular-shaped 10-wire prestressing strands were:

1. To quantify 7-wire and triangular 10-wiretransverse deformation along transfer length;
2. To evaluate the corresponding lateral strain due to Poisson's effect and assess its dependence on strand geometry and cross-sectional configuration;
3. To compare the Poisson's ratio between standard helical 7-wire strands and triangular 10-wire strands;
4. To determine the influence of Poisson's effect of strands on the radial and circumferential stress fields developed in the surrounding concrete;
5. To investigate the relationship between Poisson's ratio of strands and bond development, especially in the transfer length region;
6. To support the development or validation of analytical models for prestress transfer that incorporate Poisson's ratio of strand and its interaction with the concrete confinement.

4 Experimental program

4.1 Specimens

The strands (1770 MPa) used in simple pull-out tests are shown in Table 1 and presented in Figure 4:

- 7-wire strand, configuration 1·(3.2 mm) + 6·(3.05 mm);
- 10-wire strand, configuration 1·(2.6 mm) + 6·(2.6 mm) + 3·(2.6 mm);

Table1. Strand properties

Strand type	Inner wire [mm]	Outer wire [mm]	Strand configuration	Strand diameter d_b[mm]	Strand perimeter P_p[mm]	Area A_p[mm^2]	Pitch p[mm]
7 wire	3.2	3.05	1+6	9.3	38.280	51.85	150.00
10 wire	2.6	2.6	1+6+3	11.6	44.920	53.07	150.00

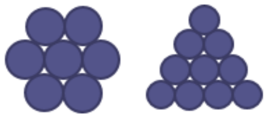

Figure 4. Geometry of tested strands: (left) standard, seven-wire; (right) ten-wire

For further considerations the following relationships have been adopted (for both types of strand):

- f_{pu} (ultimate prestress),
- f_{pt}= 0.8· f_{pu} (tensioning prestress),
- f_{pi}= 0.9· f_{pt} (initial prestress),
- f_{pe}= 0.8· f_{pt} (effective stress).

4.2 Test procedure

The experimental program involved applications of direct and indirect methods to quantify both longitudinal and lateral strains along the prestressing strand.

All measurements were synchronized with the loading system to ensure temporal consistency. Tensile testing was conducted on a single specimen of each strand type, with ten repeated measurements performed per specimen to enhance statistical validity (the five cleanest repetitions are adopted as the relevant). Specimens were mounted between the upper and lower grips of a universal testing machine, ensuring precise axial alignment. Prior to the main loading phase, the strands were straightened by initiating downward movement of the lower crosshead, applying a preload corresponding to an approximate stress of ~ 50 MPa. This initial loading step was implemented to remove slack and establish consistent baseline conditions for all tests. Minor signal fluctuations observed from the extensometers were deliberately excluded from the analysis, as they were deemed insignificant and did not adversely affect the accuracy or repeatability of the mechanical measurements.

The combination of pointwise (strain gauges) and full-field (Digital image correlation– DIC) data facilitated cross-validation of results and enabled detailed investigation of local effects at strands.

4.2.1 Direct measurement method (extensometers)

With the direct measurement method, the Poisson's ratio of strands is determined using direct measuring of specimen strains. This was accomplished through repeated tensile testing of both strand types using a universal testing machine (capacity 1000 kN) at the IGM 'KABAS' laboratory in Teslić. Because of frame and grip possibilities, specimen length was L_0= 700 mm. The experimental setup is illustrated in Figure 5.

Two extensometers were employed and arranged orthogonally: the first was positioned parallel to the strand axis to measure longitudinal deformation, while the second was modified to be mounted perpendicular to the strand to capture lateral changes in the cross-section, (Figure 5).

The longitudinal strain was calculated as:

$$\varepsilon_l = \frac{-\Delta L}{L_0}, \tag{12}$$

where ΔL is the change in gauge length and L_0 is the initial gauge length.

The lateral strain (diametric strain) for 7-wire strand was determined as:

$$\varepsilon_r = \frac{-\Delta d_b}{d_b}, \tag{13}$$

where Δd_b is the change in strand diameter and d_b is the initial diameter.

For triangular 10-wire strand, the lateral strain was determined as:

$$\varepsilon_{r_t} = \frac{-\Delta d_{b,t}}{d_{b,t}}, \tag{14}$$

where $\Delta d_{b,t}$ is the change in measurable diameter of the perpendicular setup for the triangular strand and $d_{b,t}$ is the measurable diameter of the perpendicular setup for the triangular strand (equal to the side of the triangular cross section).

The Poisson's ratio of strands (*v*) was then defined as the ratio of lateral (diametric) to longitudinal strain:

$$\nu_p = \frac{\varepsilon_r}{\varepsilon_l}, \ \nu_p = \frac{\varepsilon_{r_t}}{\varepsilon_{l_t}} \tag{15}$$

Figure 6 provides close insight into the direct measurement of lateral strain in both 7-wire and 10-wire strands during axial tensile loading. The schematic illustrates the measurement principle based on changes in the external diameter of the strand cross-section. The left side of the figure shows the setup used for the triangular 10-wire strand (nominal diameter 11.6 mm), where the lateral deformation is measured over a fixed gauge length smaller than the nominal strand diameter (this length is equal to the length of the triangular side ~ 10.45 mm). The same configuration was applied for the standard 7-wire strand (nominal diameter 9.3 mm), shown on the right; however, in this case, the strand diameter corresponds to the entire measurable gauge length, providing full contact with the lateral measurement device. This setup enables reliable assessment of lateral deformation during axial loading, which is critical for characterizing the strand's transverse mechanical response.

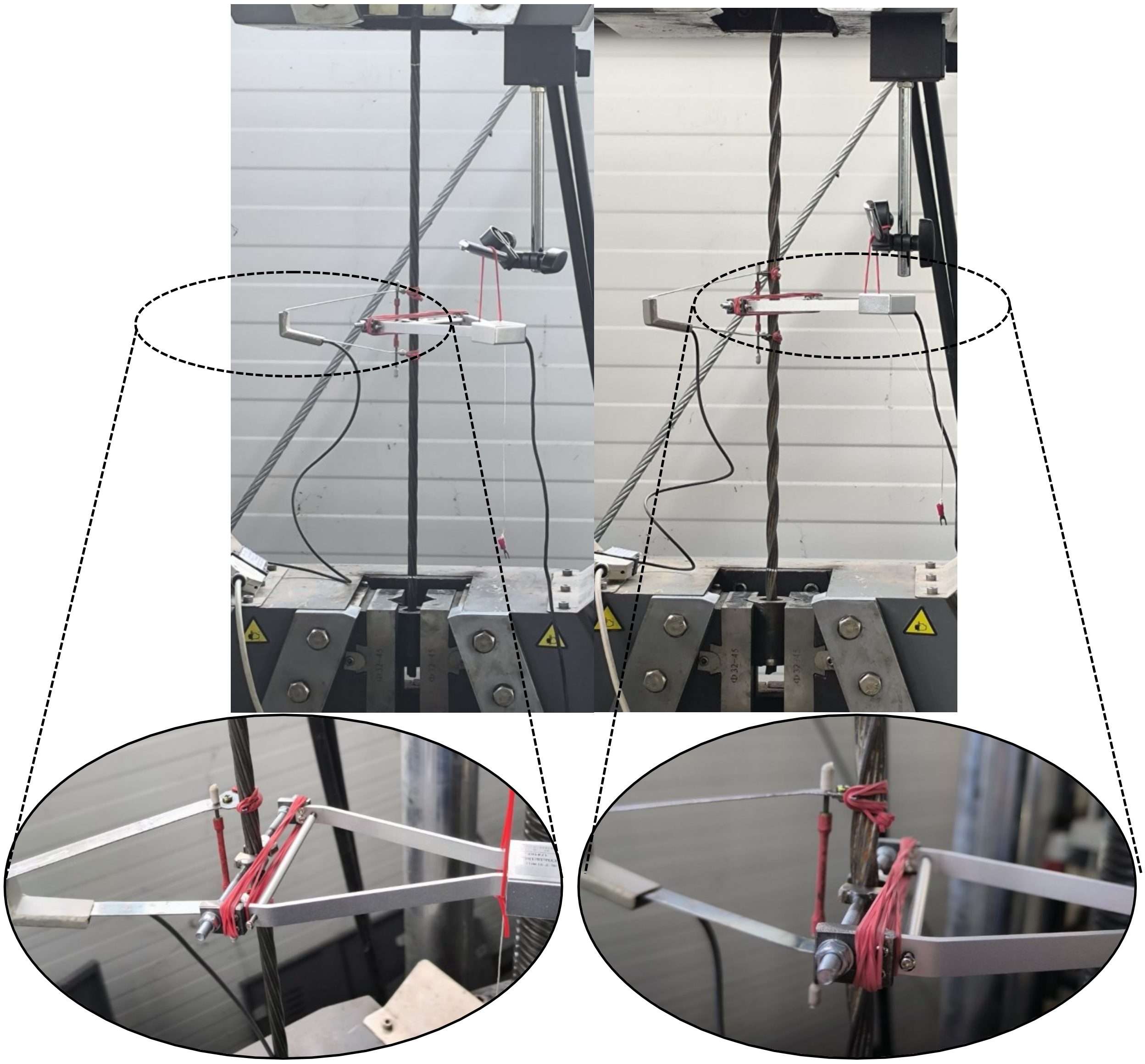

Figure 5. Direct Poisson's ratio test for strands–simultaneously x and y strain measuring: (left) standard, 7-wire 9.3mm strand; (right) triangular 10-wire 11.6mm strand

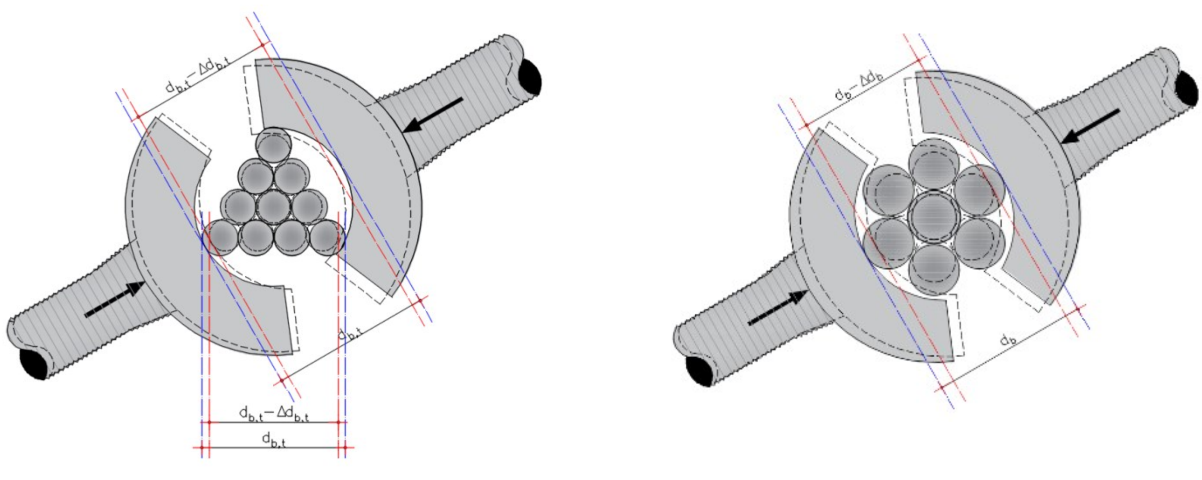

Figure 6. Schematic view of direct lateral strain measuring: (left) triangular 10-wire 11.6mm strand; (right) standard, 7-wire 9.3mm strand

4.2. Indirect measurement method (DIC)

Figure 7 presents a detailed laboratory setup designed for the indirect measurement of Poisson's ratio of a strand under axial loading conditions. At the center of the setup is a universal testing machine, equipped with mechanical grips and steel assemblies (setup for strand chucks) for axial tension testing of a prestressing strand specimen. Because of machine limits specimen length was L_0= 500 mm. The specimen is instrumented optically, without contact sensors, to enable full-field surface displacement monitoring.

A Digital Image Correlation (DIC) system is used as the core of the indirect measurement method. The system includes two high-resolution industrial cameras, each mounted on a stable tripod at an optimized angle to capture the lateral surfaces of the strand. Illumination is provided by two LED light sources placed symmetrically to minimize shadows and reflections on the strand surface, which is coated with a stochastic speckle pattern to facilitate accurate tracking by the DIC algorithm.

Two laptops are shown in the setup, one for controlling the universal testing machine, and the other for DIC acquisition and postprocessing (using software Xsight AlphaDic). Real-time displacement data are recorded during the tensile test, and post-processed to extract longitudinal and lateral displacements of the strand surface, which are interpreted as a result of elongation and contraction due to the Elasticity modulus, Poisson's effect of the material and internal rearrangement of helical wires.

This indirect method allows evaluation of Poisson's ratio of a strand without physical contact or embedding sensors into the strand, making it especially suitable for complex geometries like multi-wire strands, where direct radial measurement is difficult. The method also ensures that the mechanical behavior of the strand remains undisturbed throughout the loading process.

To facilitate accurate non-contact deformation tracking via DIC, the surface of the strand was prepared with a high-contrast random speckle pattern (Figure 8). This involved the application of a uniform matte white base coat, followed by the deposition of fine black speckles using a controlled fine spray technique. The resulting stochastic grayscale texture provides a statistically unique pattern necessary for the DIC algorithm to detect and track local displacements across the surface with sub-pixel resolution. The speckle size and distribution density were carefully calibrated to match the spatial resolution of the imaging system and the gauge length of interest, ensuring optimal correlation performance. Importantly, the applied pattern remains mechanically passive and does not interfere with the material's structural response, enabling accurate assessment of strand dilation and surface strain fields during tensile loading.

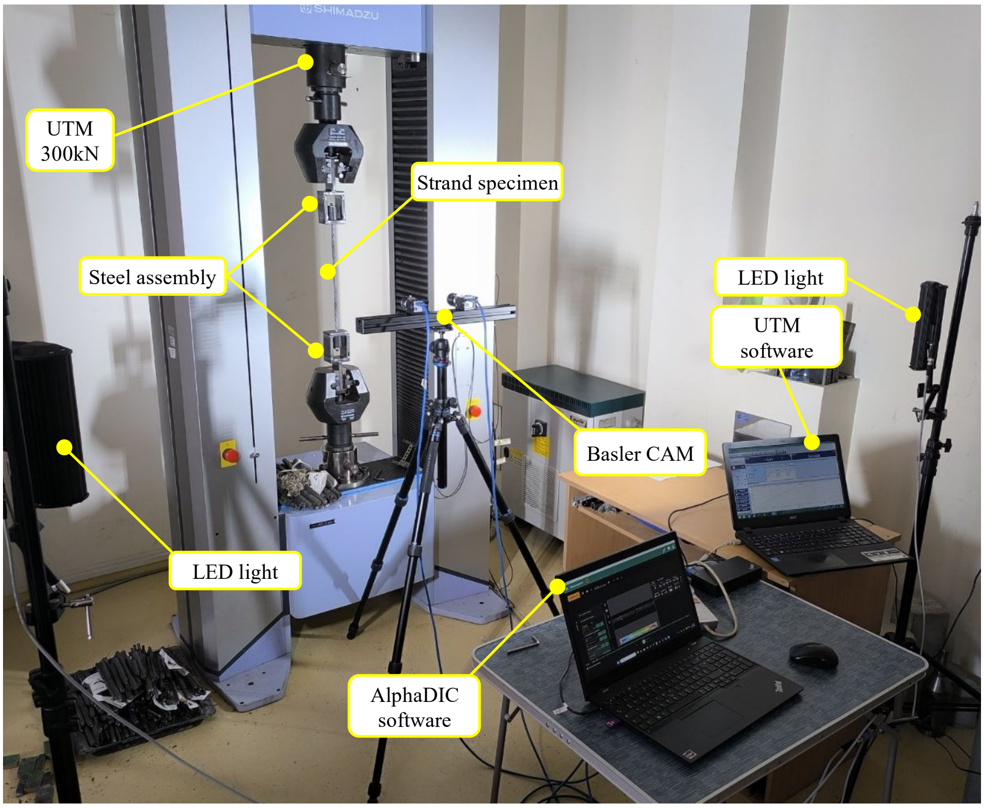

Figure 7. Indirect dilation test (DIC) – experiment setup

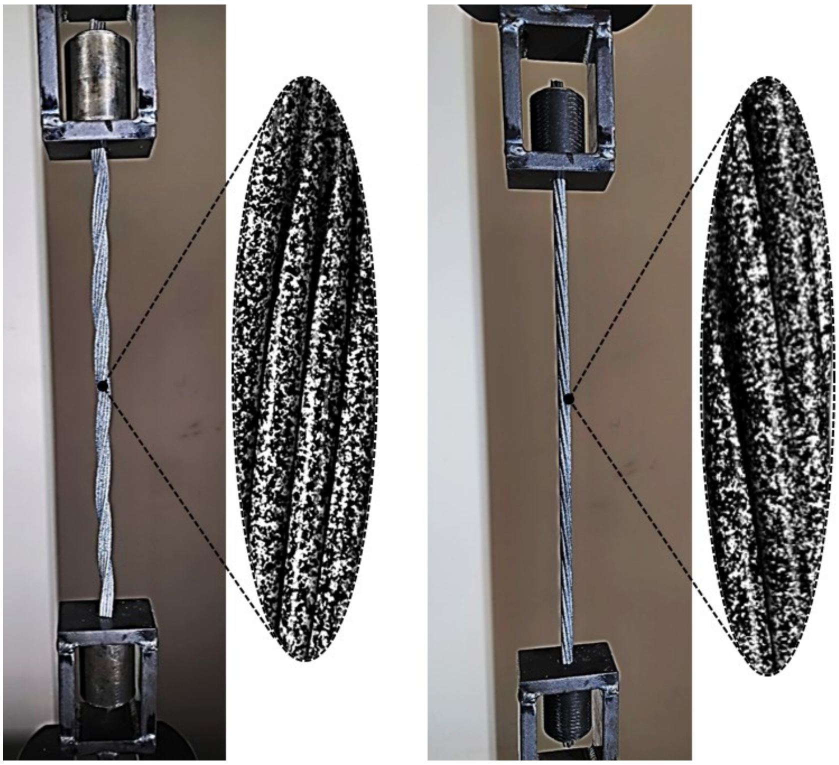

Figure 8. Stochastic speckle pattern on the strand surface

5 Experimental results

The following sections present the experimental outcomes for each testing approach (direct and indirect). Results are structured according to measurement type, starting with global responses obtained from direct testing, followed by detailed strain fields captured by DIC.

5.1 Direct measurement method

The axial stress–strain response of a triangular 10-wire and conventional 7-wire prestressing strand under uniaxial tensile loading, showing both longitudinal strain (ε_x) and lateral strain (ε_y) components obtained from five repeated tests (denoted 01–05), are presented in Figures 9 and 10, respectively. The longitudinal strain curves exhibit highly consistent behavior across repetitions (the elastic range), with all ε_x responses following a well-defined linear path beyond the initial load uptake, indicating a stable axial stiffness. The average axial stiffness was approximately E ≈204 GPa for 10-wire and E ≈197 GPa for 7-wire strands, with CoV (coefficient of variation) across both tests below 1.25%, demonstrating strong consistency and repeatability.

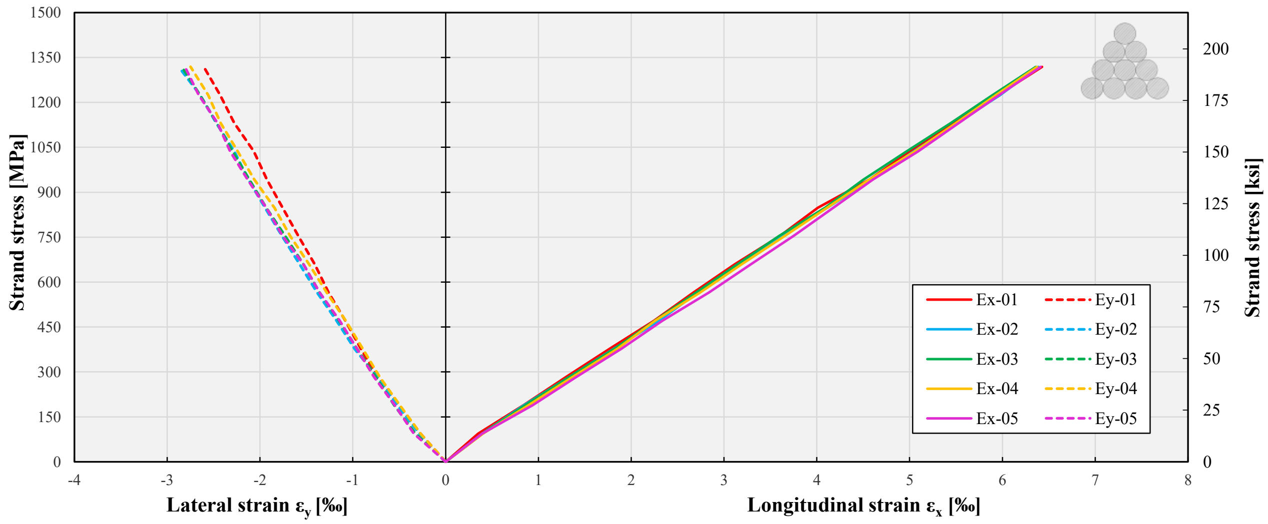

Figure 9. Direct test method –Axial stress vs strain responses of triangular 10-w 11.6 mm strand: (left side) lateral strain ε_y and (right side) longitudinal strain ε_x

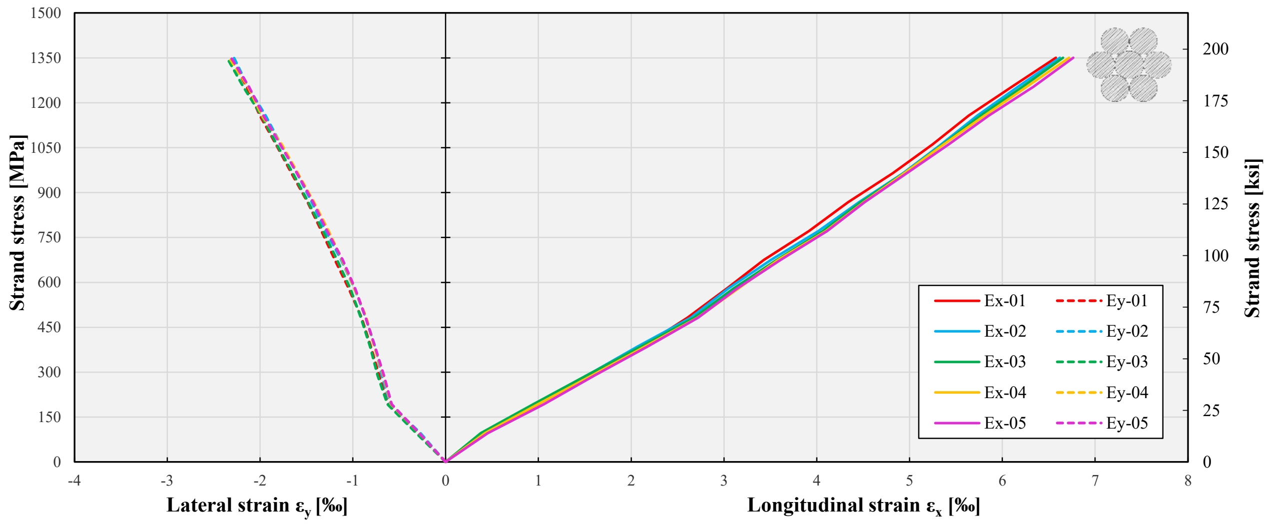

Figure 10. Direct test method –Axial stress vs strain responses of standard 7-w 9.3 mm strand: (left side) lateral strain ε_y and (right side) lateral strain ε_x

The lateral strain (ε_y) curves show a similar trend, albeit with some small nonlinear regions and slightly higher variability in the early loading stages. This scatter is associated with the sensitivity of lateral diameter-based measurement techniques and minor differences in wire engagement within the strand. The lateral response initially deviates from linearity due to internal realignment of the helical outer wires. Once full engagement is achieved, ε_y progresses linearly with ε_x, reflecting a typical Poisson's contraction behavior. The average Poisson's ratio estimated from the linear portion of the $\varepsilon_y/\varepsilon_x$ slope was $v \approx 0.44$ and $v \approx 0.34$ for 10-wire and 7-wire strands, respectively.

5.2 indirect measurement method

Figures 11 and 12 show the axial stress-strain curves obtained from Digital Image Correlation (DIC) measurements for a triangular 10-wire and conventional 7-wire prestressing strand, respectively. The longitudinal strain curves (ε_x) are consistent across all five tests, confirming stable and repeatable results when using the non-contact optical method. The average elasticity modulus from these curves was approximately E ≈208 GPa and E ≈ 202 GPa for 10-wire and 7-wire strands, respectively. The CoV in both cases was below 1.0%, which demonstrates that DIC can provide reliable axial strain measurements comparable to strain gauges.

The lateral strain curves (ε_y), also measured by DIC, display more scatter (generally the lateral strains are measured with digital area probes to capture logical small lateral deformations). This variation is caused by the tiny magnitude of lateral deformation, which makes it more sensitive to image noise, surface pattern quality, and lighting conditions. Despite the scatter, the general trend of lateral contraction is still visible, and at higher loads the curves tend to align better. The calculated Poisson's ratio of strands was $v \approx 0.45$ and $v \approx 0.33$ for 10-wire and 7-wire, respectively.

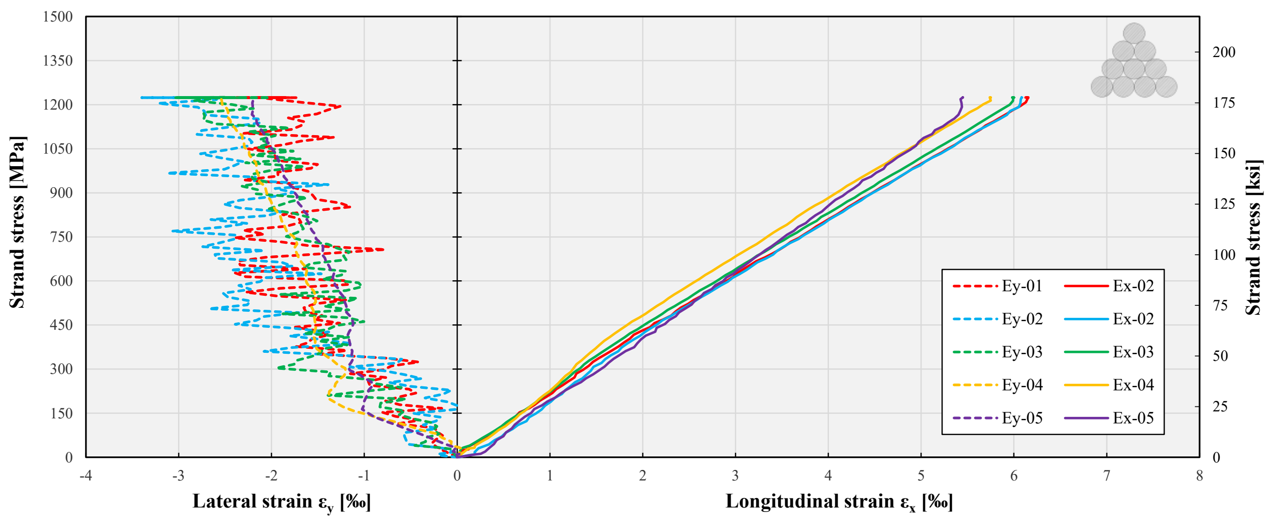

Figure 11. DIC test method – Axial stress vs strain responses of triangular 10-w 11.6 mm strand: (left side) lateral strain ε_y and (right side) lateral strain ε_x

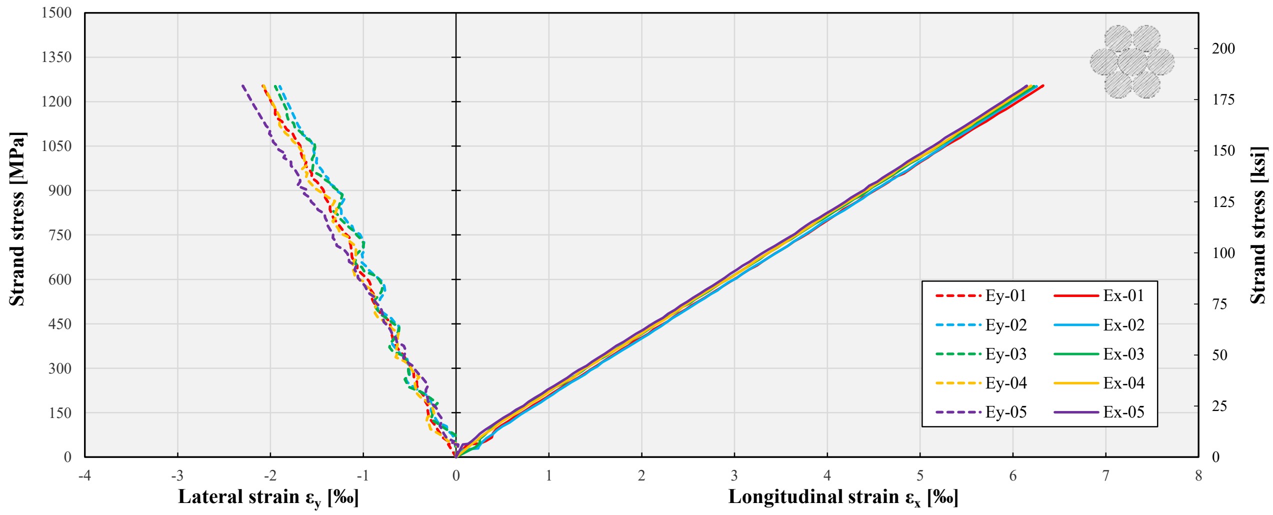

Figure 12. DIC test method – Axial stress vs strain responses of standard 7-w 9.3 mm strand: (left side) lateral strain ε_y and (right side) lateral strain ε_x

6 Analysis and discussion

The comparison between the average axial strains (ε_x) and transverse strains (ε_y) obtained from Digital Image Correlation (DIC) and the direct strain measurement approach reveals a high level of agreement for both components within the elastic range of the 10-wire strand (Figure 13). The elastic slopes extracted from the initial linear region correspond to average strain sensitivities of E ≈ 208.39 GPa for DIC and σ ≈ 204.09 GPa for the direct test method, indicating very small differences in the elastic modulus results between these two approaches. The DIC-derived ε_x curve (solid black) closely follows its direct measurement counterpart (solid red) across the full range of imposed strains, while the ε_y component (dashed lines) exhibits slightly higher scatter in the middle domain due to local surface irregularities and out-of-plane effects inherent in the optical method.

Figure 14 represents a comparison between the average axial strains (ε_x) and transverse strains (ε_y) obtained from Digital Image Correlation (DIC) and the direct strain measurement approach for the 7-wire strand. As in the previous case, again it reveals a high level of agreement for both methods within the elastic range. The elastic slopes correspond to average strain sensitivities of σ ≈ 202.23 GPa for DIC and σ ≈ 196.91 GPa for the direct test method, indicating tiny differences in the elastic modulus results between the two approaches.Based on the results, it is clearly visible that the approximately circular geometry of the 7-wire strand cross-section is more acceptable for DIC measurement of lateral strains compared to the 10-wire strand with a triangular cross-section.

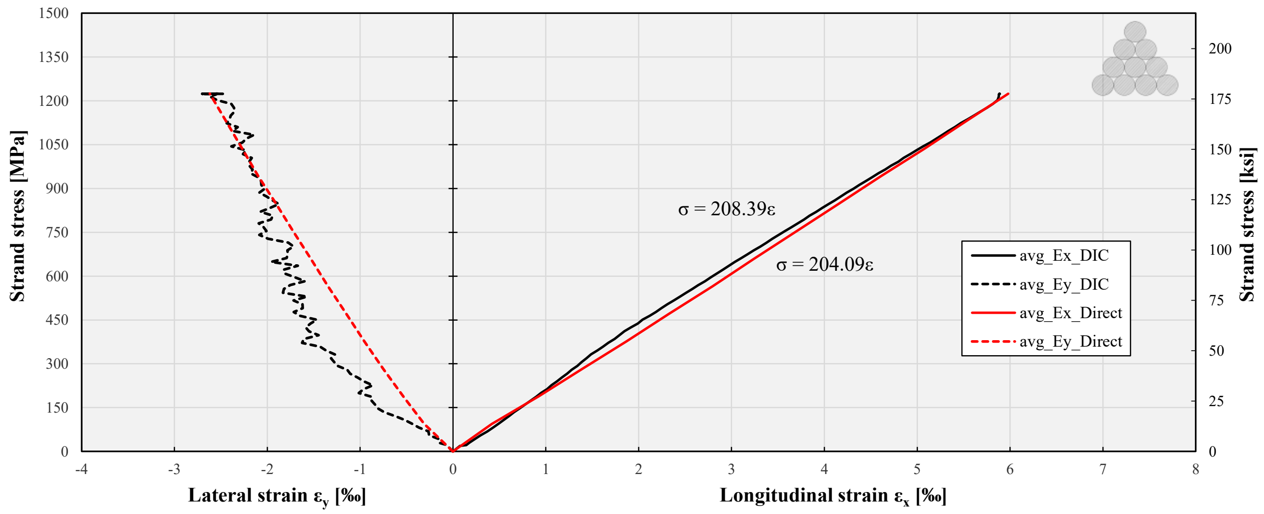

Figure 13. Comparison between direct and indirect (test) method for triangular 10-w 11.6 mm strand: (left side) lateral strain ε_y and (right side) longitudinal strain ε_x

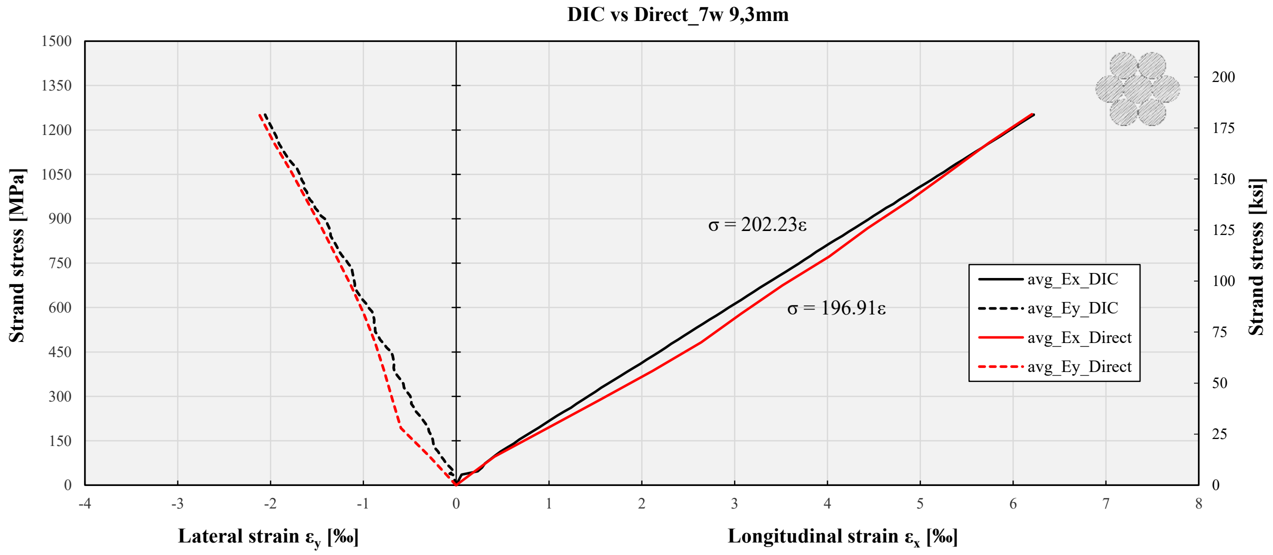

Figure 14. Comparison between direct and indirect (test) method for standard 7-w 9.3 mm strand: (left side) lateral strain ε_y and (right side) longitudinal strain ε_x

Figure 15 presents a comparative scatter plot illustrating the distribution of data points for two types of strands across two different acquisition methods: The direct test method and Digital Image Correlation (DIC). The x-axis represents Poisson's ratio of strands, while the y-axis corresponds to a strand stress. The color and shape coding within the legend differentiates between the datasets: red triangles represent 10-wire, 11.6 mm (Direct), blue squares show 10-wire, 11.6 mm (DIC), black triangles depict 7-wire, 9.3 mm (Direct), and yellow squares signify 7-wire, 9.3 mm (DIC).

Two major clusters are visually highlighted with blue ellipses, denoting zones of "average field" behavior (range of f_{se}) for each group. These clusters reflect consistent mechanical responses across the tested specimens and suggest a stable regime within each working width and acquisition type. The DIC-based measurements (yellow and blue squares) show greater scatter at lower y-axis and higher x-axis values, possibly indicating sensitivity to surface noise, edge effects, or out-of-plane deformations that DIC is particularly prone to under certain conditions. Conversely, the Direct measurement method (red and black triangles) displays a tighter distribution, which may reflect a more localized measurement approach, offering less susceptibility to field variability.

These findings emphasize the importance of acquisition technique when evaluating structural behavior under loading conditions. The DIC approach offers a broader view and captures more field-based variability, which is beneficial for mapping heterogeneous responses. However, this comes with increased data scatter. In contrast, Direct measurements provide more consistent readings, making them preferable for precise point-based evaluations, albeit at the cost of spatial insight. Ultimately, both methods offer complementary advantages, and the selection should depend on the monitoring goals and whether high-fidelity local response or full-field deformation tracking is prioritized.

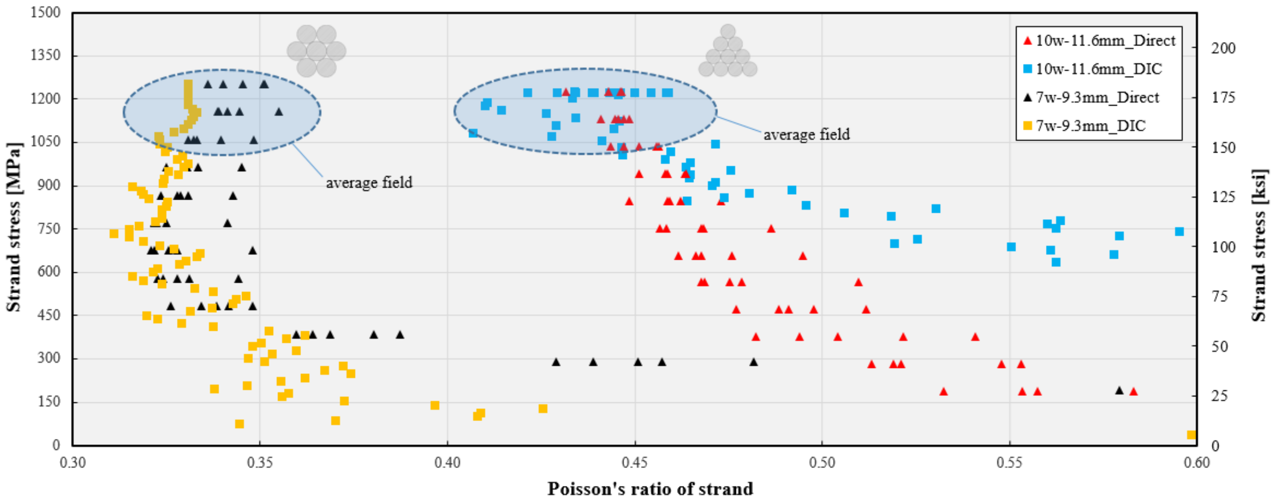

Figure 15. The Poisson's ratio of strands: direct and indirect (test) method for both type of strands

A comparative summary of the average Poisson's ratio of strand results (from average fields in Figure 15) for all examined strand types, derived from both experimental approaches, is provided in Figure 18. The bar chart distinctly compares Poisson's ratio values across five test repetitions (T-01 to T-05) for the two strand types and two test methods: Direct and Digital Image Correlation (DIC).

The 10-wire configurations consistently exhibit higher Poisson's ratio values across all test cases compared to the 7-wire counterparts, regardless of the measurement approach. This trend underscores the influence of strand configuration on the deformation response.The strands with a bigger number of wires exhibited greater lateral strain under equivalent conditions. The average Poisson's ratio for the 10-wire strands is indicated by a dashed line at 0.44, whereas the 7-wire strands average at 0.33, highlighting a significant reduction of approximately 25% in the Poisson's response for the strand type with a smaller number of wires. The reason for this lies in the specific strand configuration of 10-wire strands. The triangular-shaped 10-wire strand gives a configuration of 10 wires arranged in a triangular shape, compact and tangentially touching the adjacent. This arrangement gives 3 wires, 6 wire-wire contacts and 3 annular spaces more than in the case of 7-w strands.

Notably, for each test (T-01 to T-05), the difference between Direct and DIC measurements remains relatively small, suggesting strong consistency and reliability between the two methods. However, the Direct method tends to yield slightly higher Poisson's ratio readings in certain cases (e.g., T-02 and T-05), likely due to localized sensitivity and reduced averaging effects.

The relatively small CoV (1-8%) across all test cases, reinforces the repeatability of the deformation behavior and confirms the statistical robustness of the findings. The observed Poisson's ratio variation between strand types also supports the hypothesis that strand geometry plays a pivotal role in strain distribution and transverse expansion under load. The clear demarcation of average Poisson's ratio values via horizontal dashed lines emphasizes the global mechanical behavior distinction between the two strand configurations.

Collectively, these results validate the experimental methodology and provide critical insight into the influence of strand width and measurement technique on dilation behavior. The complementary use of DIC and Direct methods enhances confidence in the data and supports a more comprehensive understanding of the material's strain field evolution.

Figure 16 also shows that the tested results fit logically with available results from [5] for the 7-wire strands, 12.7 and 15.2 mm in diameter.

6.1 Application of the results through a numerical example

Distributions of radial and circumferential stresses in the strand–concrete interface region during prestress transfer, calculated for the release end ($z = 0,\ f_{pz} = 0$) and transfer length end ($z = L_t,\ f_{pz} = f_{pe}$) of a pretensioned concrete member are shown in Figures 17 and 18. The results were obtained using the numerical procedure defined in Eqs. (1)–(4) of [4, 5]. The input parameters on strands (diameter, modulus of elasticity, wire arrangement, initial prestress, and Poisson's ratio) were derived from our own and experimental investigations in [5], ensuring correspondence between measured strand parameters and stress distributions. Necessary data on concrete and steel properties (concrete cover, strength, cracking stress and Poisson's ratio, as well as steel Poisson's ratio) were adapted from [5].

Table 2 presents experimental data for strands from this research and Brierr's [5] data. Numerical example includes 7-wire strands (d_b= 9.3, 12.5 and 15.2 mm) and a 10-wire strand d_b=11.6 mm.

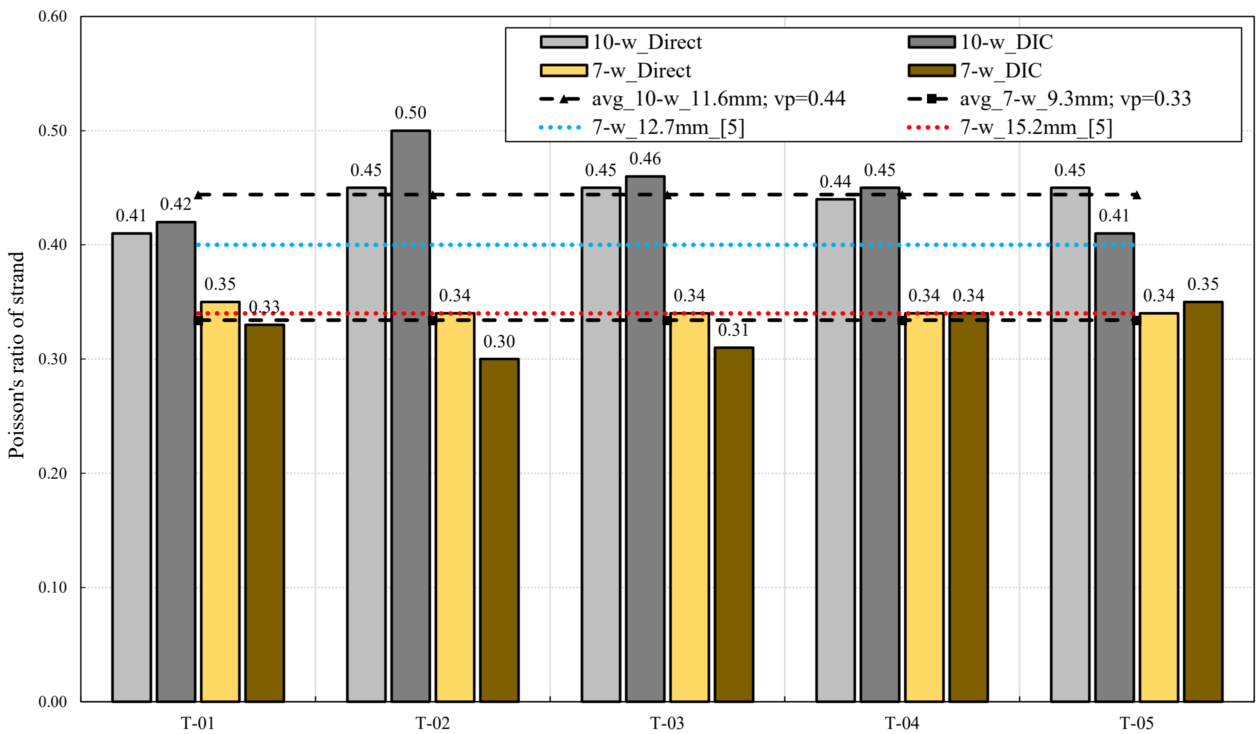

Figure 16. Average values for Poisson's ratio of strand results for Direct and DIC approaches

Table 2. Input data for numerical demonstration

Type	Diameter d_b[mm]	Radius r_o[mm]	Concrete cover[#] +r_0 c[mm]	Concrete strength f_c[MPa]	Cracking stress f_{cr}[MPa]	Young's modulus E_c[MPa]	Young's modulus E_p[MPa]	Poisson ratio of conc. v_c	Poisson ratio of steel v_s	Poisson ratio of strand v_p
7 wire	9.3*	4.65	44.7	40[#]	3.2[#]	30041.6[#]	199570*	0.17[#]	0.27[#]	0.33*
	12.7[#]	6.35	46.3				215000[+]			0.40[+]
	15.2[#]	7.6	47.6				201000[+]			0.34[+]
10 Wire	11.6*	5.8	45.8				206240*			0.44*

Note:

- *own tests; [+] tested in [5]; [#]adoptedfrom numerical example in [5];
- f_{pu} =1860 MPa → f_{pt} =0.8f_{pu}→ f_{pz} =f_{pe} =0.8f_{pt} = 1190.40 MPa;
- axial stress in concrete at z → $f_{cz} = f_{pz}r_o^2/c^2$;

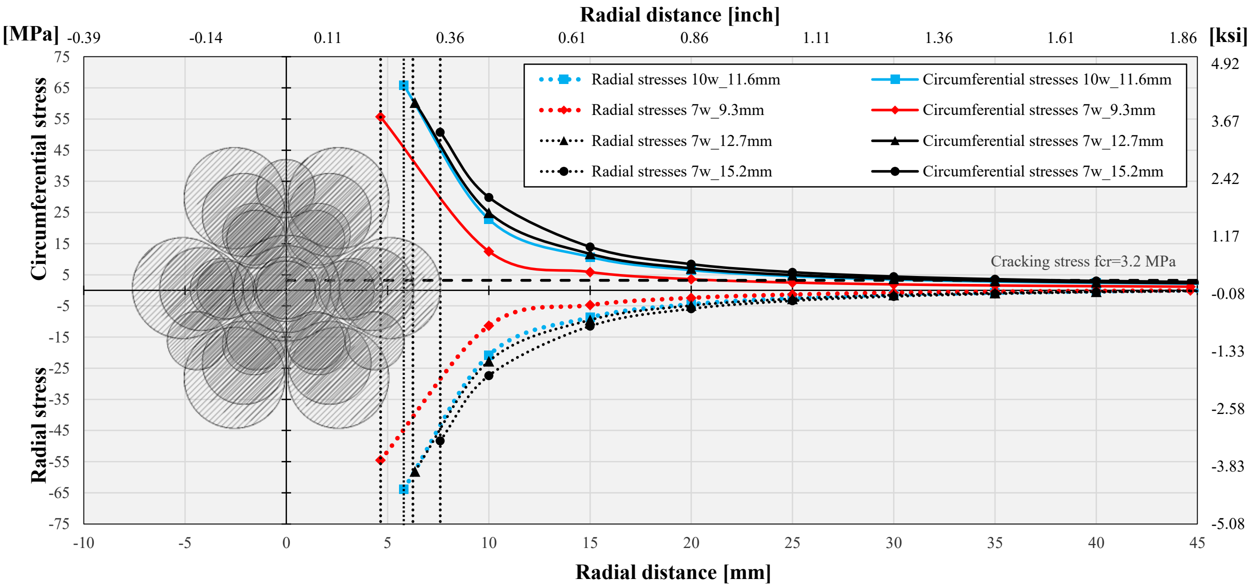

Figure 17. Variation of radial and circumferential stresses for different type of strands in radial direction incorporating experimentally derived values (z = 0)

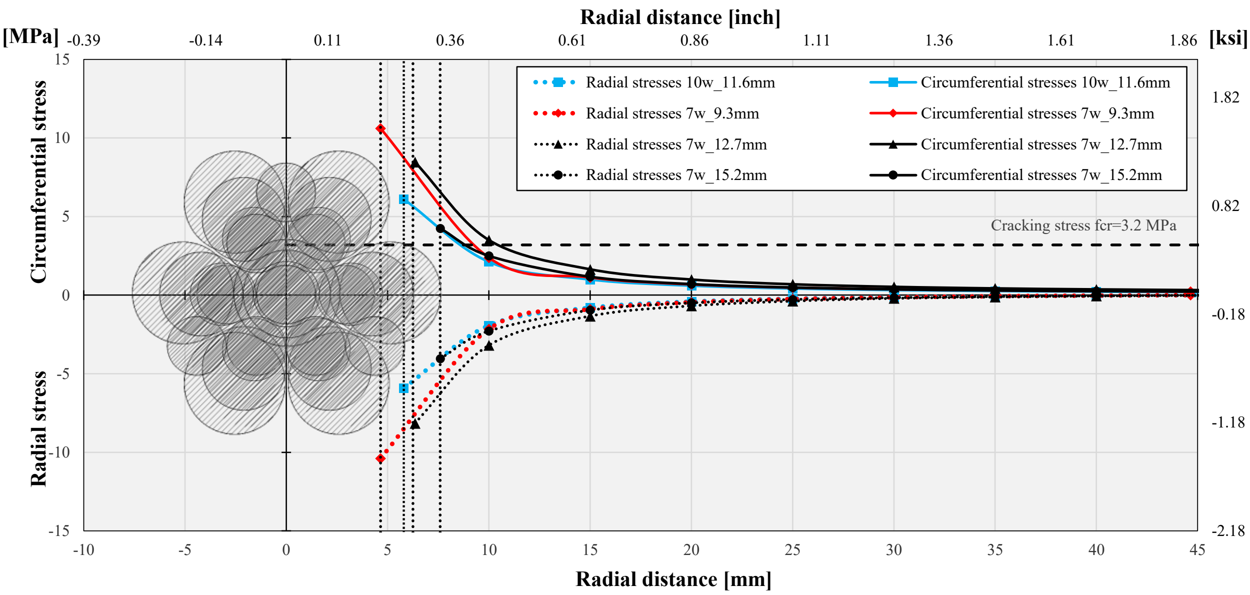

Figure 18. Variation of radial and circumferential stresses for different type of strands in radial direction incorporating experimentally derived values (z = L_t)

The numerical results for the member end zone (z = 0) show that, for both strand types and all treated diameters, the radial and circumferential stresses in the surrounding concrete vary from ~ 48to ~65 MPa (Figure 17). For 7-wire strands with 9.3 mm diameter and 10-wire strands with 11.6 mm diameter, the circumferential tensile stress in the concrete reaches the cracking threshold at approximately 20 and 30 mm, respectively, from the center of the strand. In comparison, this cracking stress is reached at approximately 30 mm for both strands, for larger 7-wire strands of 12.5 mm and 15.2 mm diameter.

For calculation of the transfer length L_t, equation (8) was used (with an asummed value η_p=2.50 for triangular 10-w strand). Transfer length for the conventional 7-wire strands was calculated with standard recommendations given in the European guideline [14], but for the innovative triangular 10-wire strand, L_t was calculated with a diameter equvivalent to the actual area (Table 1) of the strand derived from equation (5b) (→ $d_{b,eq}$ = 9.66 mm) and with tendon area parameter α_2 = 0.15 (this is explained later in subchapter 6.2). Considering the transfer length end zone (z = L_t), the results show that stresses are in the range of ~ 4 to ~ 10.5 MPa (Figure 18). All strands reach the cracking threshold at~ 8 to ~10 mm from the center of the strand.

Figure 19 shows the distribution of radial and circumferential stresses along the transfer length. It can be noticed that immediately after prestress release, radial stress reaches peak compressive values at the member end due to the maximum locked-in elastic expansion and the absence of slip, and then decreases exponentially along the transfer length as strand–concrete slip progresses and confinement demands are reduced.

The circumferential (hoop) stresses, develop tangentially around the strand perimeter as a reaction to the radial expansion forces. Their distribution reflects the local confinement efficiency of the concrete and the redistribution of stresses due to progressive bond mobilization. Near the release end of member, circumferential stresses exhibits high values (cracked zone >f_{cr}) that are directly correlated with the maximum radial stresses; further along the transfer length, circumferential stresses progressively diminish approaching the uncracked zone <f_{cr} at the strand–concrete interface (Figure 19).

Compared to conventional 7-wire strands, the 10-wire configuration exhibits substantially higher initial radial and circumferential stresses immediately after prestress release (f_{pz}= 0) and decreases to lower stresses near the strand-concrete interface at transfer length end (f_{pz}= f_{pe}). This behavior is primarily attributed to the higher strand Poisson's ratio, v_p = 0.44, observed in the 10-wire configuration, which exceeds that of 7-wire strands with diameters of 9.3, 12.7, and 15.2 mm. The strand Poisson's ratio differences range from 10% to 25% in favor of the 10-wire design, resulting in radial and circumferential stresses (at z = 0) that are increased by approximately 5 to 15 MPa when applying a triangular 10-wire strand of 11.6 mm diameter.

From previous observations, it may be concluded that the interaction of radial and circumferential stress distributions can provide a mechanical basis for explaining the variations in transfer length and initial slip between strands with different surface geometry.

By explicitly modelling both radial and circumferential stress components, rather than considering only average bond stresses, this representation captures the three-dimensional confinement mechanism that governs the initial transfer of prestress from strand to concrete.

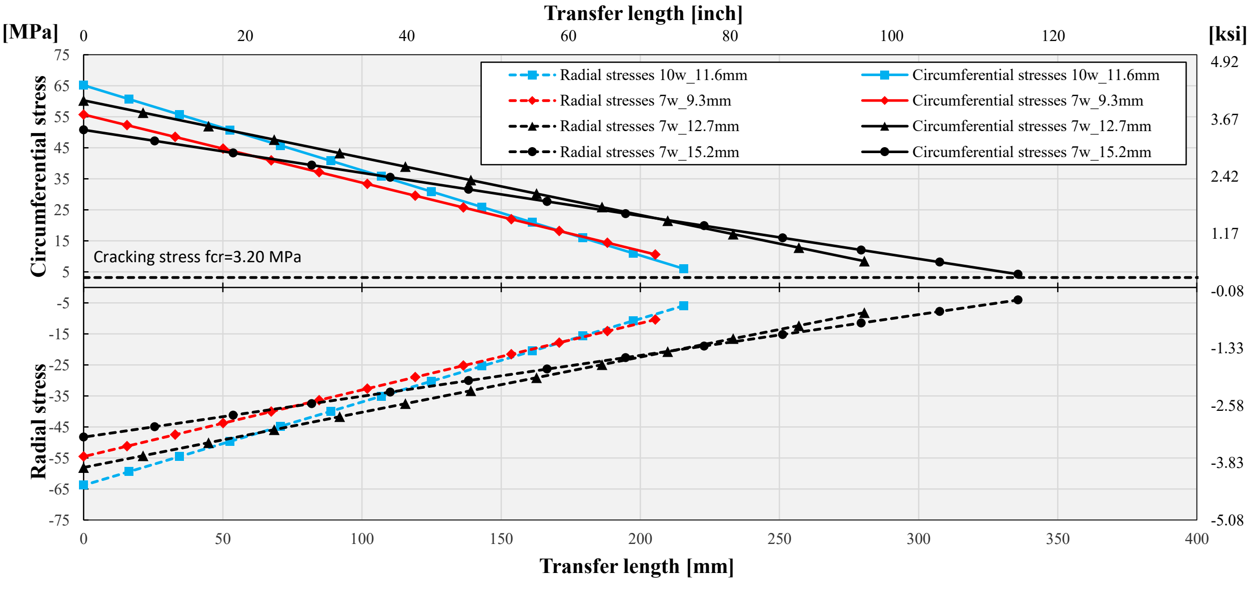

Figure 19. Variation of radial and circumferential stresses for different type of strandsalong transfer length incorporating experimentally derived values

6.2 Comparison to european standard [14]

Using equation (11) for tendon area parameter $\alpha_2$for triangular 10-wire strand we have:

- A_{actual} = 53.07 mm^2 (Table 1)
- P_{actual} = 44.
- 92 mm (Table 1)

$$correct \rightarrow \alpha_2 = \frac{A_{actual}}{P_{actual}}\frac{1}{d} = \frac{53.07}{44.92}\frac{1}{d_o} = \\ = 0.102 \rightarrow \alpha_2 \approx 0.10\,, \quad (16)$$

$$adopted \rightarrow \alpha_2 = \frac{A_{actual}}{P_{actual}}\frac{1}{d} = 0.15 \rightarrow \alpha_2 = 0.15. \quad (17)$$

The physical interpretation of the dependence of transfer length on radial stresses *p* and tendon area parameter α_2 can be summarized as follows:

- Higher radial stresses *p* increase strand-concrete friction, resulting in a shorter transfer length L_t.
- A lower tendon area parameter α_2 also leads to a shorter transfer length L_t.

This interpretation can be applied to the same type of strands. It follows that α_2 and *p* are inversely proportional.In terms of the transfer length ratio (calculated using single wires and seven-wire strands) and the ratio of Poisson's ratios, these relationships are likewise inversely proportional. For comparison, as a function of a single wire ($\alpha_{2,wire}$=0.25; ν_{wire}=0.27), this relationship can be explicitly formulated (Table 3).

Reference [5] indicates that the Poisson's ratio of a 7-wire strand is approximately 1.3 times greater than that of solid steel, with the α_2 parameter in Eq. (8) closely reflecting this relationship. Incorporating the additional result for the 9.3 mm strand, the averaged ratio of Poisson's ratios across all 7-wire strands is 0.76, which coincides with the corresponding ratio of transfer length for the 7-wire strand. This consistency provides further verification of the conclusion reported in [5].

For the tested triangular 10-wire strand, the ratio of Poisson's ratios is 0.61, which does not align with the ratio of transfer length (0.40) obtained using the unadjusted α_2 value. A similar inconsistency was observed for 7-wire strands, where calibration of α_2 from ~0.15 to ~0.19 enabled accurate representation of the Poisson's ratio relationship. By analogy with the 7-wire strand, α_2 for the 10-wire strand should be adjusted from ~0.10 to ~0.15 to match the exact ratio of Poisson's ratios between a single wire and the 10-wire configuration.

Finally, the transfer length equation (8) requires the inclusion of an additional α_2 parameter value to account for the behavior of radial stresses in the case of 10-wire strands. For this application, the recommended value is α_2=0.15. Along with this inclusion, the nominal diameter should be corrected with an equivalent diameter (equation (5b) → $d_{b,eq}$ = 9.66 mm) in relation to the actual cross-sectional area, because the diameter is a function of the actual area. Accordingly, equation (8) from [14] can be expressed as:

$$L_t = \alpha_1 \boldsymbol{\alpha_2} f_{pe} \boldsymbol{d_b} / \boldsymbol{\eta_p} \eta_1 f_{ctd(t)} [MPa, mm], \quad (18)$$

where is

α_1= 1.0 for gradual or α_1= 1.25 for sudden prestress force release,

α_2= 0.25 for plain tendons,α_2= 0.19 for 7-wire strand **and α_2= 0.15 for 10-wire strand***,

η_p= 2.7 for indented wires,η_p= 3.2 for 7-wire strand and **η_p~ 2.5 for triangular shaped 10-wire strand****,

η_1= 1.0 for good bond condition and η_1= 0.7 otherwise.

Note:

- * use d_b as equivalent diameter $\mathbf{d_{b,eq}}$ in function of the actual area of strand $A_{p,actual}$= 0.725πd_b^2/4;
- ** assumed inferior bond behavior of triangular shaped 10-wire strand through η_p- parameter.

Based on this formulation, the transfer length of a 10-wire strand is expected to be approximately 5-10% lower than that of a 7-wire strand (this can be seen in Figure 19). The expansion evidences a lower bond efficiency for the triangular 10-wire strand, yet confirms its comparable behavior to the conventional 7-wire strand.

Considering the different envelope geometry of the triangular 10-wire strand, it is recommended that the η_p parameter be calibrated relative to the 7-wire strand through a comparison of their unstressed pull-out capacities, to accurately reflect the transfer length. This adjustment of the η_p parameter is considered in this work only as an assumed value based on parallel simple pull-out tests.

7 Conclusion

On the basis of the experimental results and analytical evaluation, the principal conclusions can be summarized as follows:

1. The triangular 10-wire strand consistently shows higher Poisson's ratio values (≈0.44) than the 7-wire strand (≈0.33), indicating an approximately 25% increase in lateral strain response;
2. This effect arises from the triangular configuration of the 10-wire strand, which introduces additional wire-to-wire contacts and annular spaces compared to the 7-wire arrangement;

Table 3. Ratios of transfer length and Poisson's ratios

Strand type	Diameter d_b[mm]	Asummed α_2	Correct α_2	Ratio of transfer length		Poisson's ratio ν_p	Ratio of Poisson's ratios	
				$\frac{\alpha_{2,adopt}}{\alpha_{2,wire}}$	$\frac{\alpha_{2,corr}}{\alpha_{2,wire}}$		$\frac{\nu_{wire}}{\nu_{p,strand}}$	$\frac{\nu_{p,7-wire.9,3}}{\nu_{p,10-wire}}$
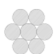	9.30	0.19	0.15	0.76	0.60	0.33	0.82	0.75
	12.70					0.40	0.68	
	15.20					0.34	0.79	
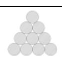	11.6	0.15	0.10	0.60	0.40	0.44	0.61	

3. The radial and circumferential stresses in the surrounding concrete exhibits higher value of ~ 65 MPa (end zone z = 0) in the case of 10-wire 11.6 mm strand compared to 7-wire strands 9.3, 12.7, 15.2 mm, with stress values of 55, 60 and 48 MPa, respectively;
4. At transfer length end (f_{pz}= f_{pe}), the 10-wire configuration exhibits lower stresses near strand-concrete interface compared to conventional 7-wire strands;
5. Using 10-wire strands, the equation (8) should therefore be extended with calibrated α_2 values: 0.25 for plain tendons, 0.19 for 7-wire strands, and 0.15 for 10-wire strands.
6. In the case of triangular 10-wire strands, equation (8) should be used not with nominal diameter, but with equivalent diameter corresponding to the actual area of the strand.
7. To accurately reflect the transfer length for triangular-shaped 10-wire strands, it is necessary that η_p parameter be calibrated relative to the 7-wire strand through a comparison of their unstressed pull-out capacities.

These findings provide a framework for an alternative approach to prestressed concrete design, offering better insight into the use of prestressing force and thereby enhancing the serviceability of structural elements.

Credit authorship contribution statement

According to the Contributor Role Taxonomy (CRediT)guidelines, the authors contributed to this work as follows:

- Žarko Lazić: Writing – Original Draft; Preparation; Conceptualization; Methodology; Formal Analysis; Data curation; Visualization;
- Veljko Koković: Writing – Review & Editing; Supervision;
- Snežana Marinković: Writing – Review & Editing; Supervision.

Declaration of competing interest

The authors declare that they have no known competing financial interests or personal relationships that could have appeared to influence the work reported in this paper.

Acknowledgment

This work was approved by patent owner Company „Armasteel Technology“ and supported by the Ministry of Scientific-Technological Development, Higher Education and Information Society of the Republic of Srpska, Faculty of Architecture, Civil Engineering and Geodesy University of Banja Luka, Faculty of Civil Engineering University of Belgrade, and a few local individuals and private companies. This support is gratefully acknowledged.

References

[1] Hoyer, E. (1939) Der-Stahlsaitenbeton. Otto Elsner Verlagsgesellschaft.

[2] Zaretsky, L. M., Kharitonov, V. A. and Dryomin, Y. A. (2012) 'United States Patent Application US 2012 / 01240548 A1 Patent Application Publication'.

[3] Lazić, Ž., Marinković, S., Koković, V., Broćeta, G., Latinović, M.'Testing bond behavior of an innovative triangular strand: experimental setup challenges and preliminary results' Building Materials and Structures 65(2022) 93-103, doi: 10.5937/GRMK2203093L.

[4] Hwan Oh, B., Sung Kim, E. and Cheol Choi, Y. (2006) 'Theoretical Analysis of Transfer Lengths in Pretensioned Prestressed Concrete Members', Journal of Engineering Mechanics, 132(10), pp. 1057–1066. doi: 10.1061/(asce)0733-9399(2006)132:10(1057).

[5] Briere, V., Harries, K., Kasan, J. and Hager, C. (2013) 'Dilation behavior of seven-wire prestressing strand-The Hoyer effect', Construction and Building Materials. Elsevier Ltd, 40, pp. 650–658. doi: 10.1016/j.conbuildmat.2012.11.064.

[6] Osborn, A., Lanier, M., & Hawkins, N. (2021). Bond of prestressing strand to concrete. PCI Journal, 66(1), 28–48. https://doi.org/10.15554/pcij66.1-04.

[7] Osborn, A. E. N., Lawler, J. S. and Connolly, J. D. (2008) 'Acceptance Tests for Surface Characteristics of Steel Strands in Pre-Stressed Concrete Appendix a: Review of Strand Bond Literature', (10).

[8] European Committee for Standardization (CEN). (2005). EN 1993-1-1: Eurocode 3: Design of steel structures – Part 1-1: General rules and rules for buildings. Brussels: CEN.

[9] Zia, P. and Mostafa, T. (1977) 'Development Length of Prestressing Strands.', J Prestressed Concr Inst, 22(5), pp. 54–65. doi: 10.15554/pcij.09011977.54.65.

[10] Martin, D.R., & Scott, B.D. (1991). Bond of prestressing strand in pretensioned concrete girders. PCI Journal, 36(5), 34–45.

[11] ACI 318-08. Building code requirements for structural concrete and commentary. American Concrete Institute, Farmington Hills, MI; 2008.

[12] Moustafa, S. (1974) 'Pullout Strength of Strand and Lifting Loops', Technical Bulletin 74-B5, Concrete Technology Corporation, Washington.

[13] Arnold, M. L. (2013) Un-tensioned pullout tests to predict the bond quality of different prestressing reinforcements used in concrete railroad ties. Manhattab, Kansas: Kansas State University.

[14] EN-1992-1-1: (2004) 'EUROCODE 2: Design of concrete structures', European Standards.

[15] J.R. Marti-Vargas, C.A. Arbelaez, P. Serna-Ros, J. Navarro-Gregori, L. Pallares-Rubio (2006) 'Analytical model for transfer length prediction of 13 mm prestressing strand', Structural Engineering and Mechanics, Vol. 26, No. 2, 211-229.